J. Appl. Comput. Mech., 6(1) (2020) 171-182
DOI: 10.22055/JACM.2019.28273.1473

ISSN: 2383-4536
jacm.scu.ac.ir

M&MoCS
Shahid Chamran University of Ahvaz

Journal of Applied and Computational Mechanics

Research Paper

Entropy Generation of Variable Viscosity and Thermal Radiation on Magneto Nanofluid Flow with Dusty Fluid

Hiranmoy Mondal[1], Shweta Mishra[2], Prabir Kumar Kundu[3], Precious Sibanda[1]

[1] *School of Mathematics, Statistics and Computer Science, University of KwaZulu-Natal*
Private Bag X01 Scottsville, 3209, South Africa, Email: hiranmoymondal@yahoo.co.in

[2] *Amity Institute of Information Technology, Amity University*
NewTown, Kolkata, West Bengal 700135, India, Email: shweta9935@gmail.com

[3] *Deptartment of Mathematics, Jadavpur University*
West Bengal, Kolkata 700032, India, Email: kunduprabir@yahoo.co.in

Received January 17 2019; Revised April 03 2019; Accepted for publication April 05 2019.
Corresponding author: Hiranmoy Mondal (hiranmoymondal@yahoo.co.in)

Abstract. The present work illustrates the variable viscosity of dust nanofluid runs over a permeable stretched sheet with thermal radiation. The problem has been modelled mathematically introducing the mixed convective condition and magnetic effect. Additionally analysis of entropy generation and Bejan number provides the fine points of the flow. The of model equations are transformed into non-linear ordinary differential equations which are then transformed into linear form using the spectral quasi-linearization method (SQLM) for direct Taylor series expansions that can be applied to non-linear terms in order to linearize them. The spectral collocation approach is then applied to solve the resulting linearized system of equations. The validity of our model is established using relative entropy generation analysis. A convergence schematic was obtained graphically. Consequence of various parameters on flow features have been delivered via graphs. Some important findings reported in this study that entropy generation analysis have significant impact in controlling the rate of heat transfer in the boundary layer region. The paper acquires realistic numerical explanations for rapidly convergent solutions using the Spectral quasi-linearization method. Convergence of the numerical solutions was monitored using the convergence graph. The initial guess values are automatically satisfied the boundary conditions. The resulting equations are then integrated using the Spectral quasi-linearization methods. The influence of radiation, heat and mass parameters on the flow are made appropriately via graphs. The effects of varying certain physical parameters of interest are examined and presented.

Keywords: Spectral quasiliearization method; Viscous dissipation; Variable viscosity; Entropy generation; Thermal radiation.

1. Introduction

Nanofluid is a broad range of engineering application and used to enhance the heat transfer and energy efficiency in various kinds of thermal systems. The main applications of nanofluids include thermal storage lubrications drillings diesel combustions domestic refrigerators chiller solar water heating biomedicine (in cancer therapy) nuclear system cooling defense space electronic cooling and transportation (engine cooling/ vehicle thermal management) etc. In recent years, nanofluids have attracted a considerable amount of interest due to their novel properties that make them

Published online: July 19 2019

potentially useful in a number of industrial applications including transportation, power generation, micro-manufacturing, thermal therapy for cancer treatment, chemical and metallurgical sectors, heating, cooling, ventilation, and air-conditioning. Makinde and Aziz [1] investigated nanofluid flow over a linear stretching sheet with thermophoresis and particle Brownian motion. They reported that stronger Brownian motion and thermophoresis lead to an increase in the rate of heat transfer. However, the opposite was observed in the case of the rate of mass transfer. Thereafter, Wang and Majumdar [2] and Pramuanjaroenkij [3] investigated the thermal conductivity and viscosity of nanofluids theoretically and experimentally.

The magnetohydrodynamic boundary layer flow through a stretching surface has been examined or past two decades because of their huge applications n various manufacturing and engineering processes such as food processing industries textiles polymers etc. Pal and Mondal ([4], [5]) discussed the buoyancy effects on MHD incompressible fluid having thermal radiation and transverse magnetic field. The reduce system of nonlinear ordinary differential equations were examined by Runge Kutta integration technique. Rashidi et al. [6] studied magnetohydrodynamics boundary layer flow of viscoelastic fluid via a moving surface. Rashidi and Erfani [7] discussed the steady MHD flow because of a rotating disk possessing the sound effects of ohmic heating and viscous dissipation.

The effect of thermal radiation on boundary layer flow and heat transfer processes is of major importance in the design of advanced energy convection systems which operate at high temperature. Thermal radiation occurring within these systems is usually the result of emission from the hot walls and the working fluid. Thermal radiation effects become more important when the difference between the surface and the ambient temperature is large. Pal and Chatterjee [8] studied the effects of chemical reaction, heat and mass transfer along a wedge with heat source and concentration in the presence of suction or injection. Kandasamy et al. ([9], [10]) presented thermophoresis and variable viscosity effects on MHD mixed convective heat and mass transfer past a porous wedge in the presence of chemical reaction. He analyzed MHD flow and mass transfer of an electrically conducting fluid of second grade in a porous medium over a stretching sheet with chemically reactive species.

The increase of temperature leads to a local increase in the transport phenomena by reducing the viscosity across the momentum boundary layer due to which heat transfer at the wall is also affected. Thus in order to predict most accurately the flow behavior, it is important and necessary to take into account the variation of viscosity with temperature. Therefore, to predict the flow and heat transfer rates it is necessary to take into account the temperature dependent viscosity of the fluid. For lubricating fluids heat generated by internal friction and the corresponding rise in the temperature affects the viscosity of the fluid and so that the fluid viscosity no longer be assumed constant. Pal and Mondal [11] investigated variable viscosity effects on MHD flow and heat transfer over a stretching sheet. Manjunatha and Gireesha [12] considered the effect of variable viscosity on the dusty flow and heat transfer from a linearly stretching sheet. Pantokratoras [13] presented further results on the variable viscosity on the flow and heat transfer to a continuous moving flat plate. The effect of thermal radiation and variable fluid viscosity on free convective and heat transfer past a porous stretching surface analyzed by Mukhopadhyay and Layek [14]. The study of heat source/sink on heat transfer is very important in view of several physical problems, i.e. non-uniform heat source/sink has significant impact in controlling the rate of heat transfer in the boundary layer region. Aforementioned studies involve heat transfer to include only the effect of uniform heat source/sink (i.e. temperature independent heat source/sink). Abel et al. [15] investigated on non-Newtonian boundary layer flow past a stretching sheet by taking into account of non-uniform heat source and frictional heating.

Entropy represents a measure of the disorder in a specified system. Entropy generation is dependent on the reversibility of a specified procedure. In an isolated system, entropy tends to increase with time, but remains steady for reversible reactions. Due to the increasing use application of nanofluids and nanoparticles in engineering and medical applications, it is important to investigate and study the influence of these nanoparticles on entropy generation on real life. Noghrehabadi et al. [16] considered entropy generation in nanofluid flow over a stretching sheet with heat generation/absorption. Sithole et al [17] investigated the entropy generation using the spectral methods. Hidouri et al. [18] and Aracely et al. [19] studied the influence of the Soret effect on entropy generation in double diffusive convection with nonlinear thermal radiation.

In many transport processes existing in nature and industrial applications in which mass transfer is a consequence of buoyancy effects caused by diffusion of chemical species. The study of such processes is useful for improving a number of chemical technologies such as in polymer production. Many practical diffusive operations involve the molecular diffusion of species in the presence of a chemical reaction within the boundary layer. The presence of a foreign mass in air or water causes some kind of chemical reaction. During a chemical reaction between two species, heat is also generated. A reaction is said to be first-order if the rate of reaction is directly proportional to concentration itself. The chemical reaction rate decreases with increasing activation energy. Further concluded that the velocity and temperature profiles increase with increasing chemical reaction rate constant for exothermic reaction, but opposite effects are found for endothermic reaction. Buoyancy and heat generation/absorption were shown to have marked effects on the boundary layer and velocity profile established by Maleque [20]. The study of the combined effects of heat and mass transfer with chemical reactions have been considered by several researcher ([21], [22], [23], [24]).

The motivation of the present study is to investigate the entropy generation analysis and Bejan number for unsteady dusty nanofluid. To the best of the authors knowledge no paper in the research has so far studied entropy generation and Bejan number in dusty nanofluid over a stretching sheet with chemical reaction. We use the proper similarity transformations have been utilized into ordinary differential equations and then solved using by Spectral quasi-linearization method (SQLM). The obtained solution has been analyzed by plotting graphs of dimensionless velocity, temperature, entropy generation and Bejan number.

2. Problem Formulation

Consider the unsteady two-dimensional MHD flow of a magneto-micropolar fluid over an nonlinear porous surface in the *xy* plane. The *x*-axis is parallel to the vertical surface and *y*-axis is perpendicular to the sheet. The flow is subject to micropolar viscous dissipation and Joule heating. Particle thermophoresis, the thermal radiation and nanoparticle Brownian motion are considered to be significant. A magnetic field of strength B_0 is exerted in a transverse trend to the flow. The uniform sheet and ambient temperatures are given by T_w and T_∞ respectively, while $C_w(x)$ is the concentration close to the sheet and C_∞ represents the ambient concentration where $C_w(x) > C_\infty$ and $T_w(x) > T_\infty$. We assumed that $U(x,t)$ is the sheet velocity, given by $ax/(1-\varepsilon t)$, $a,\varepsilon > 0$ are constants and t is the time variable. The magnetic field term is $B_0(t) = B/\sqrt{1-st}$. The system of equations for the heat and mass transfer dusty fluid in the presence of variable viscosity are given by:

$$\frac{\partial u}{\partial x}+\frac{\partial v}{\partial y}=0 \tag{1}$$

$$\frac{\partial u}{\partial t}+u\frac{\partial u}{\partial x}+v\frac{\partial u}{\partial y}=\frac{1}{\rho}\frac{\partial}{\partial y}\left(\mu\frac{\partial u}{\partial y}\right)-\frac{\sigma B_0^{\,2}}{\rho}u+g\beta_T(T-T_\infty)+g\beta_c(C-C_\infty), \tag{2}$$

$$\begin{aligned}\frac{\partial T}{\partial t}+u\frac{\partial T}{\partial x}+v\frac{\partial T}{\partial y}&=\frac{\upsilon}{C_p}\left(\frac{\partial u}{\partial y}\right)^2+\frac{1}{\rho C_p}\left(\kappa+\frac{16\sigma^* T_\infty^{\,3}}{3k^*}\right)\frac{\partial^2 T}{\partial y^2}+\frac{1}{\rho C_p}q'''\\&+\tau\left(D_B\frac{\partial T}{\partial y}\frac{\partial C}{\partial y}+\frac{D_T}{T_\infty}\left(\frac{\partial T}{\partial y}\right)^2\right)+\frac{\sigma B_0^{\,2}}{\rho C_p}u^2\end{aligned} \tag{3}$$

$$\frac{\partial C}{\partial t}+u\frac{\partial C}{\partial x}+v\frac{\partial C}{\partial y}=\frac{D_T}{T_\infty}\frac{\partial^2 T}{\partial y^2}-R(C-C_\infty) \tag{4}$$

where u is the velocity along the *x*-axis, v is the velocity along the *y*-axis, μ and ρ are the dynamic viscosity and the density of the fluid respectively, σ and B the electrical conductivity are the magnetic field strength respectively, g is the gravitational acceleration, β_T and β_C are thermal and solutal coefficients respectively. Further, $\alpha = (k_f/\rho c_p)$ is the thermal diffusion which represents the ratio between the effective thermal conductivity and the effective specific heat, $\tau = (\rho c)_p/(\rho c)_f$ is proportion between the effective heat capacity of the nanofluid and the heat capacity of the base fluid, σ^* and k^* are the Stefan–Boltzmann constant and mean absorption coefficient respectively, D_B represents the Brownian mention coefficient, Q represents the volumetric rate of heat and D_T represents thermophoretic diffusion coefficient. The auxiliary conditions are

$$\begin{aligned}&u=U_w(x,t), v=0, -k_w\frac{\partial T}{\partial y}=h_w\{T_w(x,t)-T(x,t)\}, D_B\frac{\partial C}{\partial y}+\frac{D_T}{T_\infty}\frac{\partial T}{\partial y}=0 \;\; as \;\; y=0,\\&u\to 0, C\to C_\infty, T\to T_\infty \;\; as \;\; y\to\infty.\end{aligned} \tag{5}$$

Equations (1)–(4) are reduced to a dimensionless form using the following variables,

$$\psi = x\left(\frac{a\upsilon}{1-st}\right)^{0.5} f(\eta),\ \eta=\left(\frac{a}{\upsilon(1-st)}\right)^{0.5} y,\ \varphi(\eta)=\frac{C-C_\infty}{C_w-C_\infty},\ \theta(\eta)=\frac{T-T_\infty}{T_w-T_\infty} \tag{6}$$

where prime denotes the differentiation with respect to η. The variation of temperature dependent viscosity defined as $\mu=\mu_0\exp(-\beta_1\theta(\eta))$, where μ_0 is the viscosity at temperature T_w and β_1 is variable viscosity parameter, when $\beta_1>0$ for liquid and $\beta_1<0$ for gases. The non- uniform heat source/sink q''' is modeled as

$$q'''=\frac{kU_w(x)}{\upsilon x}[A_s(T_w-T_\infty)f'+(T-T_\infty)B_s] \tag{7}$$

where A_s and B_s are the coefficients of space and temperature dependent heat source/sink respectively. When

$A_s, B_s > 0$ corresponds to internal heat generation and $A_s, B_s < 0$ corresponds to internal heat absorption. Hence, the system of equations (1)–(4) is transformed to

$$f''' + f''(f e^{\beta_1\theta} - \beta_1\theta') - Ae^{\beta_1\theta}(f' + 0.5\eta f'') - e^{\beta_1\theta} f'^2 - Ha^2 e^{\beta_1\theta} f' \\ + e^{\beta_1\theta}(\lambda\theta + \delta\varphi) = 0, \tag{8}$$

$$\frac{1+Nr}{\Pr}\theta'' + f\theta' - f'\theta - 0.5A(4\theta + \eta\theta') + Ec\, f''^2 + Ec\, Ha^2 f'^2 + Nb\theta'\varphi' + Nt\theta'^2 \\ + \frac{1}{\Pr}(A_s f' + B_s\theta) = 0 \tag{9}$$

$$\frac{1}{Le}\varphi'' + f\varphi' - f'\varphi - 0.5A(4\varphi + \eta\varphi') + \frac{1}{Le}\frac{Nt}{Nb}\theta'' - R_1\varphi = 0, \tag{10}$$

with boundary conditions are given by

$$f(0) = 0,\ f'(0) = 1, \theta'(0) = -Bi(1-\theta(0)),\ Nb\varphi'(0) + Nt\theta'(0) = 0, \\ f'(\infty) = 0, \theta(\infty) = 0, \varphi(\infty) = 0 \tag{11}$$

where primes denote the derivative with respect to η. The parameters in equations (8)–(10) are defined as

$$A = \frac{e}{a}, \lambda = \frac{g\beta_T b}{a^2},\ \delta = \frac{g\beta_c c}{a^2},\ Ha^2 = \frac{\sigma B^2}{a\rho}, \\ Nr = \frac{16\sigma^* T_\infty^3}{\kappa k^*}, Ec = \frac{U_w^2(x)}{C_p(T_w - T_\infty)} = \frac{a^2 x}{bC_p}, \Pr = \frac{\upsilon}{\alpha}, \\ Nb = \frac{\tau D_B(C_w - C_\infty)}{\upsilon}, Nt = \frac{\tau D_T(T_w - T_\infty)}{\upsilon T_\infty}, Le = \frac{\upsilon}{D_B}, Bi = \frac{h_w}{k_w}\frac{x}{\sqrt{\mathrm{Re}}} \tag{12}$$

where A is the unsteadiness parameters respectively, λ is thermal boundary parameter, δ is the concentration boundary parameter, Ha represents the magnetic parameter, Nr is radiation parameter, Ec and Pr are the Eckert number and the Prandtl number respectively, Nb represents Brownian motion parameter, Le is the Lewis number and Nt represents the thermophoresis parameter, Bi is the Biot number.

The physical quantities of interest of the problem are skin friction co-efficient, Nusselt number and Sherwood number, which are defined as

$$C_f = \frac{\tau_w}{\rho U_w{}^2},\ Nu_x = \frac{xq_w}{\kappa(T_w - T_\infty)}, Sh_x = \frac{xm_w}{D_m(C_w - C_\infty)} \tag{13}$$

where the skin friction τ_w, heat transfer q_w and mass transfer m_w are given by

$$\tau_w = \mu\left(\frac{\partial u}{\partial y}\right)_{y=0},\ q_w = -\kappa\left(\frac{\partial T}{\partial y}\right)_{y=0},\ m_w = -D_m\left(\frac{\partial C}{\partial y}\right)_{y=0} \tag{14}$$

using the non-dimensional variables, we obtain

$$C_f\,\mathrm{Re}^{0.5} = e^{-\beta_1\theta} f''(0),\ Nu_x\,\mathrm{Re}^{-0.5} = -\theta'(0), Sh_x\,\mathrm{Re}^{-0.5} = -\varphi'(0) \tag{15}$$

3. Entropy Generation

Entropy generation is a measure of the irreversibility of a procedure. The volumetric rate of local entropy generation S''_{gen}, which is obtained for two-dimensional flow as follow

$$S''_{gen} = \underbrace{\frac{k_f}{T_\infty^2}\left[1 + \frac{16\sigma^* T_\infty^3}{3k^*}\right]\left[\left(\frac{\partial T}{\partial x}\right)^2 + \left(\frac{\partial T}{\partial y}\right)^2\right]}_{S_{\backslash th}} + \underbrace{\frac{\mu}{T_\infty}\left[\left(\frac{\partial u}{\partial x}\right)^2 + \left(\frac{\partial u}{\partial y}\right)^2\right]}_{S_{dis}} + \underbrace{\frac{\sigma B_0{}^2}{T_\infty}(u^2 + v^2)}_{S_m} \\ + \underbrace{\frac{RD}{C_\infty}\left[\left(\frac{\partial C}{\partial x}\right)^2 + \left(\frac{\partial C}{\partial y}\right)^2\right] + \frac{RD}{T_\infty}\left[\left(\frac{\partial T}{\partial x}\frac{\partial C}{\partial x}\right) + \left(\frac{\partial T}{\partial y}\frac{\partial C}{\partial y}\right)\right]}_{S_{dif}} \tag{16}$$

where R is the ideal gas D is the mass diffusion. Equation (16) demonstrates that entropy generation has six contributory. The first source is irreversibility due to heat transfer as well as thermal radiation (HTI) S_{th}, the second is due to velocity of dusty fluid (S_{dis}), the third source is caused by the magnetic field (S_m) and the fourth terms are caused by mass transfer (S_{dif}). Equation (16) can be written as a sum of all the terms as

$$S''_{gen} = S_{th} + S_{dis} + S_m + S_{dif} \tag{17}$$

It is convenient to express the entropy generation (N_G) as the ratio of S''_{gen} and the rate of entropy generation (S''_0), which can be obtained as

$$S''_0 = \frac{k_f (T_w - T_\infty)^2}{T_\infty^2 x^2} \tag{18}$$

The characteristic entropy generation rate S''_{gen} gives the optimal entropy generation at which the thermodynamic performance of a system is optimized. Finding S''_{gen} requires solving an optimization problem that is constrained by the irreversible operations of the system. The physical characteristics of the system are varied until a minimum entropy generation is found. The entropy generation number is given by

$$\begin{aligned} N_G(\eta) = \frac{S''_{gen}}{S''_0} &= \mathrm{Re}(1+Nr)(\theta^2 + \theta'^2) + \frac{Br}{\chi} e^{-\beta_1 \theta}(f'^2 + \mathrm{Re}\, f''^2) + \frac{Ha^2 \Pr}{\chi}(f + \mathrm{Re}\, f'^2) \\ &+ \Sigma \left(\frac{\Omega}{\chi}\right)^2 (\varphi^2 + \mathrm{Re}\, \varphi'^2) + \Sigma \left(\frac{\Omega}{\chi}\right)(\theta\varphi + \mathrm{Re}\, \theta' \varphi') \end{aligned} \tag{19}$$

The parameters appearing in equation (19) are obtained as

$$\begin{aligned} &\mathrm{Re} = \frac{U_w(x) x}{\upsilon}, Br = \frac{\mu U_w^2(x)}{k_f \Delta T}, \Delta T = T_w - T_\infty, \chi = \frac{\Delta T}{T_\infty}, \\ &\sum = \frac{RDC_\infty}{k_f}, \Omega = \frac{\Delta C}{C_\infty}, \Delta C = C_w - C_\infty \end{aligned} \tag{20}$$

Equation (19) reveals there are four irreversibility sources that contribute to the entropy generation number. The fraction of irreversibility from each source can be found by dividing the irreversibility source by the total entropy generation number leading to non-dimensional parameters, so

$$\gamma_{th} = \frac{S_{th}}{N_G}, \gamma_{dis} = \frac{S_{dis}}{N_G}, \gamma_m = \frac{S_m}{N_G}, \gamma_{dif} = \frac{S_{dif}}{N_G} \tag{21}$$

where γ_{th} and γ_{dis} are the fractions of irreversibility due to thermal diffusion and dusty fluid viscous dissipation, respectively, γ_m and γ_{dif} are the fractions of irreversibility due to magnetic field and concentration diffusion.

As can be seen, the heat transfer irreversibility, diffusive irreversibility and magnetic field contribute in entropy generation. Therefore, it is more worth investigating under which condition, heat transfer dominates the entropy generation. To investigate this question, the Bejan (Be) number is define as the ratio entropy generation due to the heat transfer and entropy generation number

$$Be = \frac{\mathrm{Re}(1+Nr)(\theta^2 + \theta'^2)}{N_G(\eta)} \tag{22}$$

The Bejan number takes values in range [0,1]. At the extreme when Be = 1 the irreversibility of heat transfer dominates. On the other extreme when Be = 0 the combined effects of diffusion and magnetic field dominates the irreversibility. When Be = 0.5, the contribution of heat transfer in entropy generation is the same as the combined contribution of diffusion and magnetic field in entropy generation. Additionally, the Bejan number (Be) is considered at the best values of the parameters at which the entropy generation its minimum.

4. Results and Discussion

The system of equations was solved numerically using the spectral quasi-linearization method for selected parameter values. The nonlinear partial differential Eqs. (8)–(10) with the boundary conditions (11) were solved numerically using the spectral quasiliearization method for selected parameter values. The iteration is started from initial approximations which satisfy Eq. (11), namely, $f(\eta) = 1 - e^{\eta}$, $\theta(\eta) = Bi\, e^{\eta} / (1+Bi)$ and $\varphi(\eta) = -Nt\, Bi / (Nb(1+Bi)) e^{\eta}$. The relative entropy generation has four sources of irreversibility, such as thermal diffusion, dusty fluid flow, magnetic field and concentration diffusion. Figure 1 shows that the contribution of each source to the total irreversibility is illustrated as a function of distance from the surface. We note that close to the sheet all sources of irreversibility contribute positively to the total irreversibility. In the proximity of the sheet, the irreversibility caused by the thermal diffusion γ_{th} has a positive and noticeable contribution to the total irreversibility. It is dominant along the sheet due to temperature gradients and the high motion of nanoparticles. In the proximity of the sheet, the irreversibility caused by dusty fluid viscous dissipation γ_{dis} has relative influence because the velocity gradients are relative high. Away from the surface the irreversibility caused by the concentration diffusion (γ_{dif}) is the dominant source of irreversibility. The contribution of irreversibility due to thermal diffusion decreases away from the sheet due to a decrease in the temperature gradients. Further, the combined effect of the increase in the concentration diffusion and the decrease in temperature gradient leads to the dominance of this irreversibility in the regions far from the sheet. Close to the sheet, there is no contribution from the irreversibility due to the magnetic field (γ_m) to the total irreversibility.

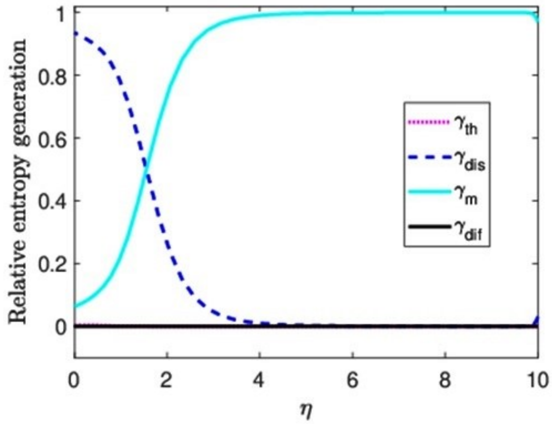

Fig. 1. Entropy generation of source irreversibility.

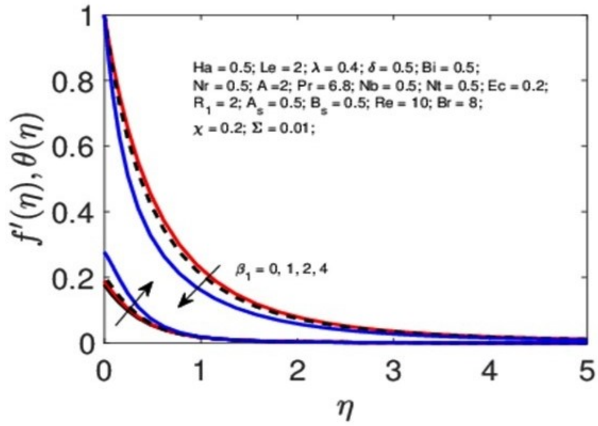

Fig. 2. Effects of variable viscosity parameter β_1 on velocity and temperature distribution.

The effect of fluid viscosity parameter β_1 on velocity and temperature profiles verses η is depicted in Figure 2. It is observed that the dusty velocity profiles decrease with an increasing values of fluid viscosity parameter β_1. This is because of the fact that with an increase in the value of dusty fluid viscosity parameter decreases in the velocity boundary layer thickness. Physically, this is because a given larger β_1 implies higher temperature difference between the surface and the ambient fluid. The increase in the value of β_1 has tendency to increase the thermal boundary layer thickness. This causes to increase the values of temperature profile that increase in the dusty viscosity parameter increases the temperature of the fluid and dust phase.

Figure 3 display results for the concentration distribution for different values of fluid viscosity parameter β_1. It is shows the variation of the dimensionless concentration profile $\varphi(\eta)$ for various values of dusty variable viscosity parameter β_1 for both air and liquid that the concentration increases very rapidly with η and its value increases with increase in β_1.

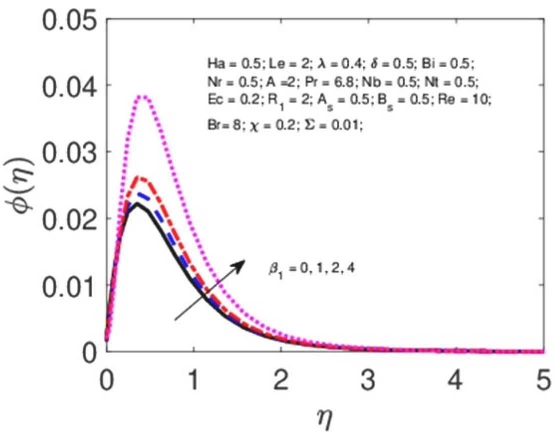

Fig. 3. Effect of variable viscosity parameter β_1 on concentration profile.

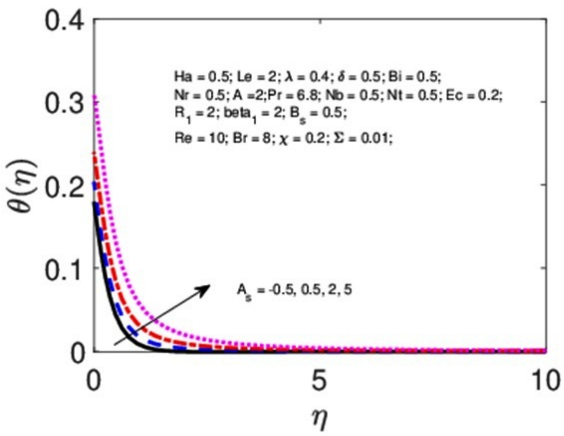

Fig. 4. Effect of non-uniform heat source/sink parameter A_s on temperature profiles.

Figure 4 depicts the effect of space-dependent heat source/sink parameter A_s. It is observed that the boundary layer generates the energy, which causes the temperature profiles to increase with increasing the values of $A_s > 0$ (heat source) where as in the case of $A_s < 0$ (absorbtion) boundary layer absorbs energy resulting in the temperature to fall considerably with decreasing in the value of $A_s < 0$. The effect of temperature-dependent heat source/sink parameter B_s on heat transfer is demonstrated in Figure 5. This graph illustrates that energy is released when B_s which causes the temperature to increase, whereas energy is absorbed by decreasing the values of $B_s < 0$ resulting in the temperature to drop significantly near the boundary layer.

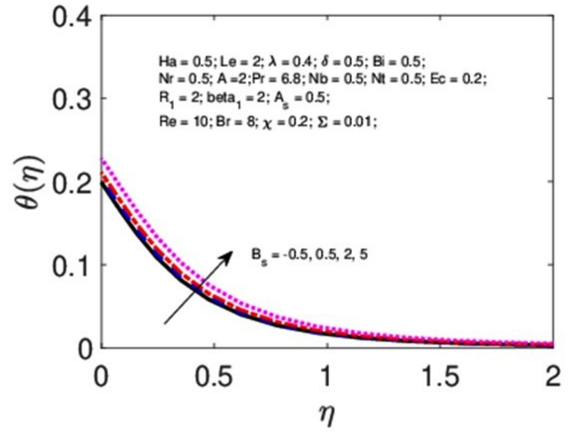

Fig. 5. Effect of temperature-dependent heat source/sink parameter B_s on temperature profiles.

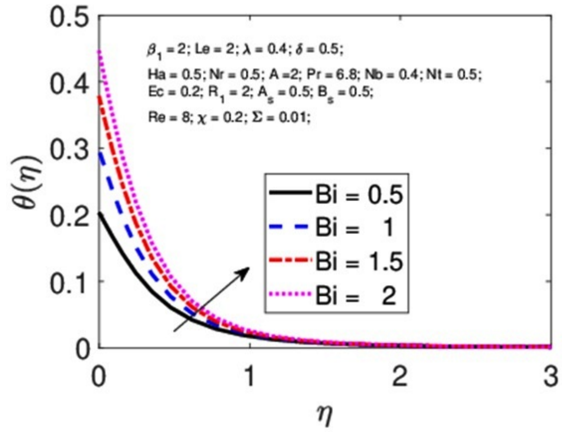

Fig. 6. Influence of Biot number on temperature profiles.

We examined the effect of Biot number *Bi* on the temperature and concentration in Figure 6. It is shown that increasing the Biot number will result in a increase in both the temperature and concentration in the boundary layer. Since we considered a plate of infinite length, this means the length scale is long enough so that the the Biot number exceed one. This implies that heat resistance offered at the surface is less than heat resistance offered within the solid plate. Temperature gradients within the solid are no longer negligible, we can no longer assume constant temperature within the solid. This is so since the plate is heated to maintain a constant temperature yet it is constantly being cooled at the surface by the fluid it comes in contact with. The transfer of thermal energy from the solid to the dusty fluid results in an increase in the thermal energy of the fluid leading to an increase in the dusty fluid temperature and concentration of the chemical species as a result of an increase in the chemical reaction. It showed that concentration increased for increasing values of the Biot number are seen in Figure 7.

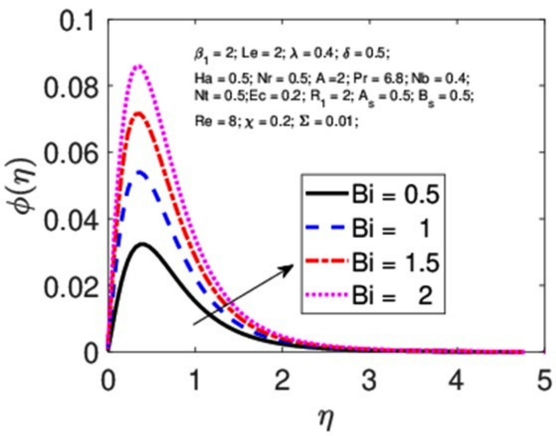

Fig. 7. Influence of Biot number on concentration profiles.

The skin-friction coefficient increases as the dusty fluid variable viscosity parameter β_1 increases, while it increases as a result of increasing the value of Brownian motion parameter *Nb*, as shown in Figure 8. The effect of the viscosity parameter on the local Nusselt number, in terms of Nu_x is displayed in Figure 9. It is observed that the local Nusselt number decreases with increasing the viscosity parameter β_1 whereas reverse trend is observed by increasing the value of the Brownian motion parameter. The influences of β_1 and *Nb* on Sherwood number are shown in Figure 10. It is observed from this figure that the effects of increasing β_1 is to increase the Sherwood number, whereas no significant effect is seen by increasing the value of the Brownian motion parameter *Nb*.

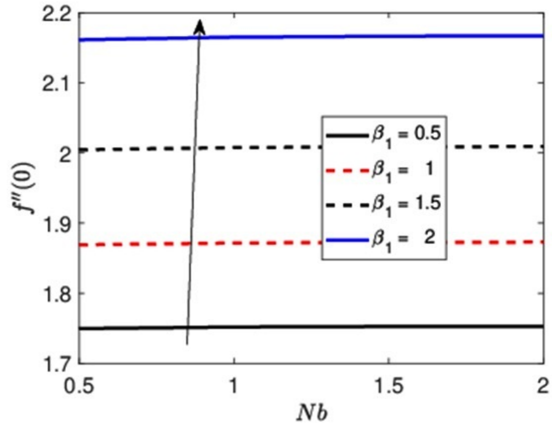

Fig. 8. Influence of viscosity parameter β_1 on the local skin friction co-efficient number.

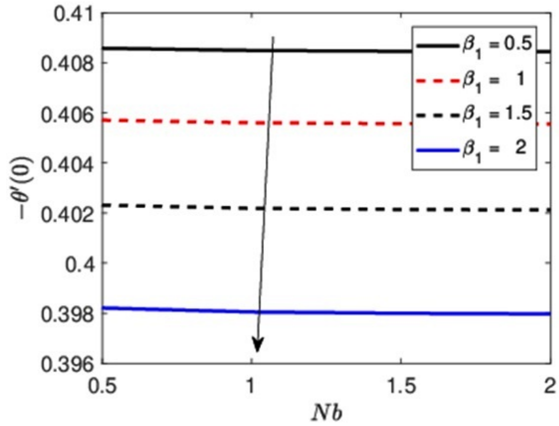

Fig. 9. Influence of viscosity parameter β_1 on the local Nusselt number.

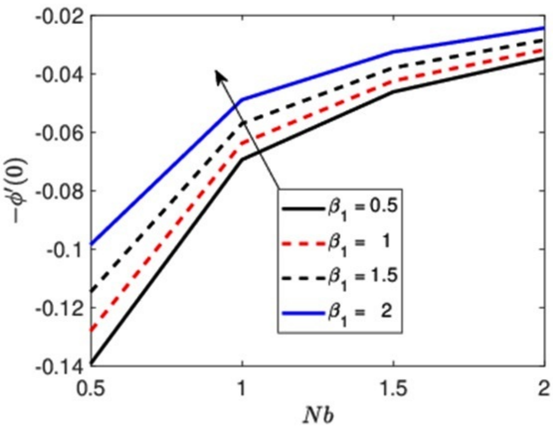

Fig. 10. Influence of viscosity parameter β_1 on the local Sherwood number.

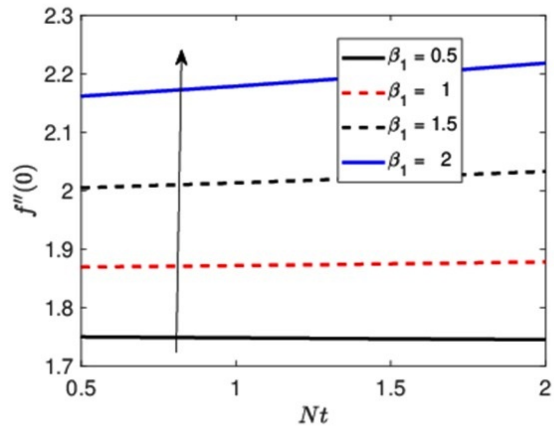

Fig. 11. Influence of viscosity parameter β_1 on the skin friction co-efficient with *Nt*.

It is observed from Figure 11 that the local skin-friction coefficient is overshoot due to increase in the viscosity parameter β_1, whereas reverse effect is observed by increasing the value of the Thermophoresis parameter. Figure 12 shows clearly that the presence of temperature dependent viscosity gives enhanced local Nusselt number, in terms of $-\theta'(0)$, in a manner that the local Nusselt number decreases as thermophoresis parameter increases. The influences of β_1 and *Nt* on Sherwood number are shown in Figure 13. It is observed from this figure that the effects of increasing β_1 is to increase the Sherwood number, whereas no significant effect is seen by increasing the value of the thermophoresis parameter *Nt*.

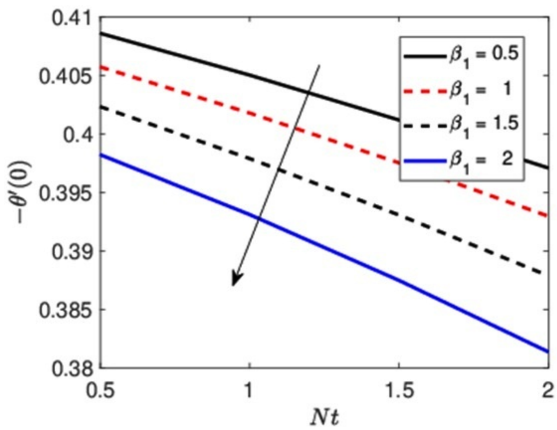

Fig. 12. Influence of viscosity parameter β_1 on the local Nusselt number with *Nt*.

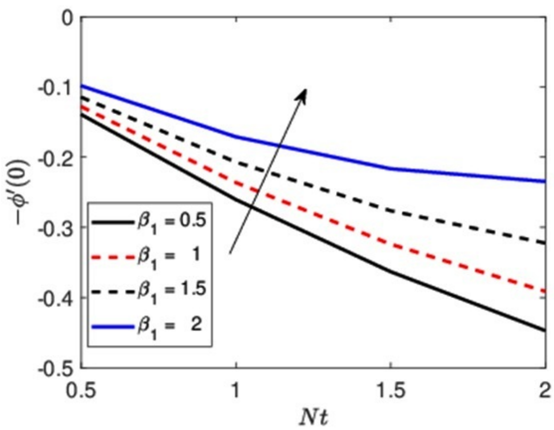

Fig. 13. Influence of viscosity parameter β_1 on the local Sherwood number with *Nt*.

The behavior of dimensionless entropy generation profile N_G represents one of the most important characteristic of this study. The variation in N_G is examined and exhibited in different figures with different values of the pertinent parameters, namely, viscosity parameter β_1, the Hartmann number *Ha*, the Reynolds number *Re* and the Brinkman number *Br*, respectively. It is worth noting that Figures 14-17 provide several ways to control the entropy generation number. Figure 14 illustrates the effect of viscosity parameter β_1 on the entropy generation number N_G, where it is seen that the entropy generation number is a decreasing function of β_1, especially close to the sheet surface. The decrease of N_G with an increase in viscosity parameter β_1 at the vicinity of the sheet can be attributed to the velocity deduction inside the boundary layer with increase in β_1. Figure 15 shows the effect of the Hartmann number *Ha* on the entropy generation number N_G. An increase in *Ha* results in the increment of N_G. In the neighborhood of the sheet vicinity, Ha has significant impact on N_G, whereas at regions far away from the sheet, the *Ha* has slight effect on N_G. This effect tends to increase the resistance of the fluid motion, consequently the heat transfer rates increase, which result in an increase in N_G. However, at far from the sheet vicinity, the influence of *Ha* is insignificant. Figure 16 relates the entropy generation number with the Reynolds number *Re*. It is noted that the *Re* has remarkable effects on N_G as an increase in *Re* leads to a significant increase in N_G, in the vicinity of the sheet. As *Re* increases, N_G caused by the heat transfer dominates N_G caused by the diffusion effect and the magnetic field in the neighborhood of the stretching sheet. This effect makes the fluid motion more random to the extent that troubled fluid motions arise. Consequently, the N_G increases due to the contribution of heat transfer. Moreover, when *Re* increases, the inertia forces are promoted, hence, the values of the viscous forces are decreased. By increasing the value of *Re*, the acceleration of the fluid increases in the vicinity of the sheet. However, far away from the sheet these effects are negligible. Figure 17 displays entropy generation with the Brinkman number, which represents a measure of the significance of the heat produced by viscous heating proportional to heat transported by molecular conduction. An increase in *Br* tends to increase N_G especially in the vicinity of the sheet. Heat generated bey viscous dissipation prevails through the heat transported via the molecular conduction in the neighborhood of the sheet. In the vicinity of the sheet, essential heat generation occurs over the boundary layer of the moving fluid particles, which trends N_G to enhance by increasing the degree of disorder of the system.

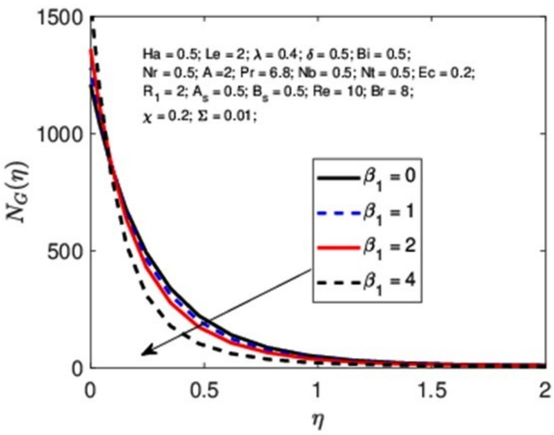

Fig. 14. Effect of viscosity parameter β_1 on the entropy generation number N_G.

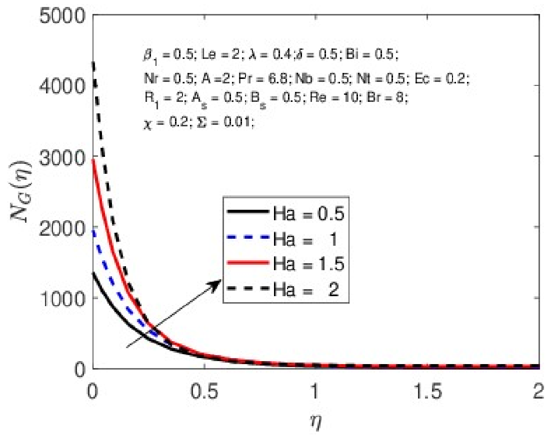

Fig. 15. Effect of Hartmann number *Ha* on the entropy generation number N_G.

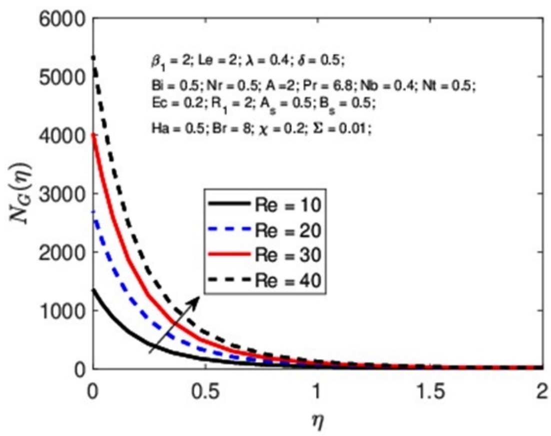

Fig. 16. Effect of Reynolds number *Re* on the entropy generation number N_G.

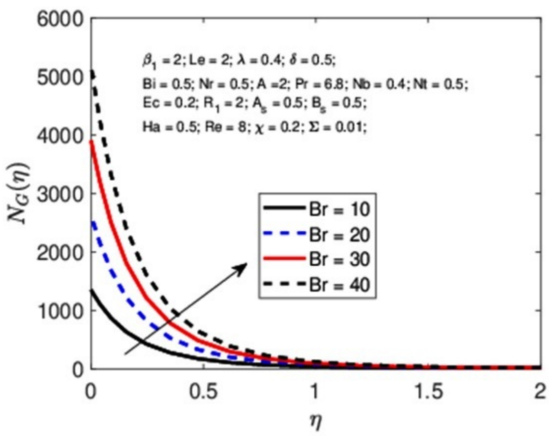

Fig. 17. Effect of Brinkmann number *Br* on the entropy generation number N_G.

The entropy generation number can be due to (the diffusion effect and magnetic field) and heat transfer. Therefore, it is legitimate to investigate which of these three factors dominates the entropy generation number. To identity whether the entropy generation due to heat transfer dominates over the entropy generation due to (diffusive irreversibility and magnetic field) (and vice versa), the Bejan number is studied for different physical parameters. Moreover, Be can be used to identity the dominant irreversibility: either the heat irreversibilit or the diffusion and the magnetic field irreversibility. The variation in the Bejan number *Be* according to the viscosity parameter β_1 are illustrated in Figures 18. It is noted that the value of *Be* increases in the neighborhood of the sheet, and it increases gradually when the distance increases from the surface of the sheet. Figure 19 illustrates that the Bejan number *Be* is proportionally related to the Hartmann number *Ha*. As *Ha* increases, the entropy generation traced to diffusive irreversibility and magnetic field is totally controlled by the entropy generation due to heat transfer at the vicinity of the sheet. Figures 20 and 21 show the variations in the Bejan number *Be* with different values of the Brinkman number *Br* and Biot number *Bi*. It is observed that an increase in *Br* and *Bi* leads to an increases in *Be*. From Equation it is note that an increase in *Br* and *Bi* contribute to the increase in the magnitude of the diffusive irreversibility with magnetic field irreversibility.

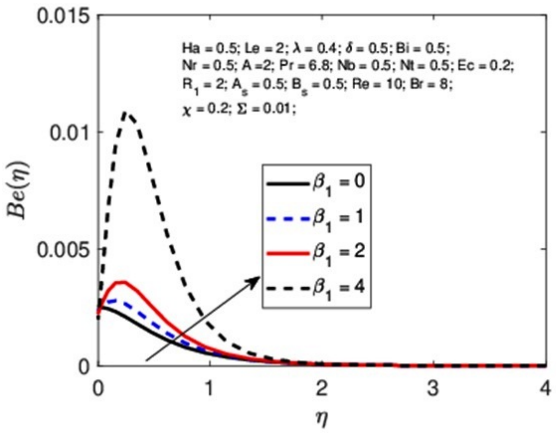

Fig. 18. Effect of viscosity parameter β_1 on the Bejan number *Be*.

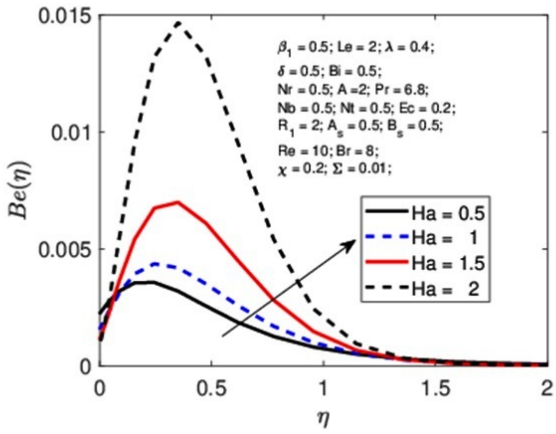

Fig. 19. Effect of Hartmann number *Ha* on the Bejan number *Be*.

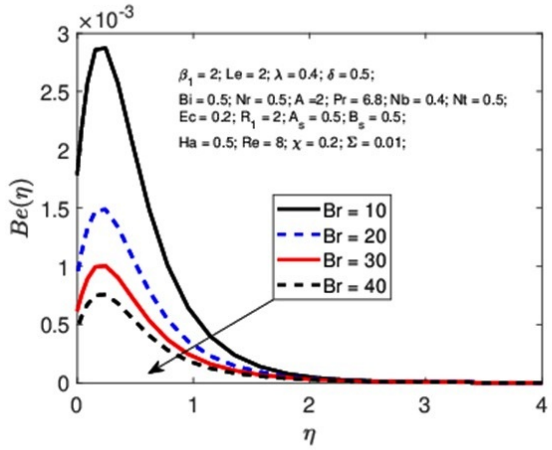

Fig. 20. Effect of Brinkmann number *Br* on the Bejan number *Be*.

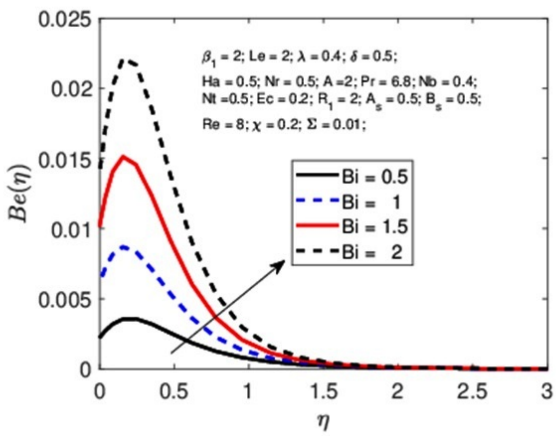

Fig. 21. Effect of Biot number *Bi* on the Bejan number *Be*.

5. Conclusion

The boundary layer continuity, momentum, energy, and concentration equations are transformed by using similarity transformations, which are solved using by the Spectral quasi-linearization method (SQLM). The important findings from the analysis include the following points:

• Enhancement occur in thermal boundary layer, whereas the concentration and momentum boundary layer reduces when the viscosity parameter increases.

• The presence of space-dependent heat source/sink parameter A_s and temperature-dependent heat source/sink parameter B_s is to increase the temperature profile.

• The entropy generation number decreases with the increase of viscosity parameter, while the entropy generation number increases with the increase of Brinkman number and Reynolds number.

• The Bejan number is strongly affected by variations in the viscosity parameter and dimensionless Brinkman groups.

• The local skin friction co-efficient and Sherwood number increase with the increase in thermophoresis parameter.

• The local Nusselt number decrease with the increase in Brownian motion parameter.

Acknowledgments

The authors are grateful to the Claude Leon Foundation Postdoctoral Research Foundation and the University of KwaZulu-Natal for financial supports.

Conflict of Interest

The authors declared no potential conflicts of interest with respect to the research, authorship and publication of this article.

Funding

The authors received no financial support for the research, authorship and publication of this article.

References

[1] O.D. Makinde, A. Aziz, Boundary layer flow of a nanofluid past a stretching sheet with a convective boundary condition, *International Journal of Thermal Sciences*, 50, 2011, 1326-1332.
[2] X.Q. Wang and A.S. Mujumdar, A review on nanofluids - part ii: Experiments and applications, *Brazilian Journal of Chemical Engineering*, 25, 2008, 631-648.
[3] S. Kakac, A. Pramuanjaroenkij, Review of convective heat transfer enhancement with nanofluids, *International Journal of Heat and Mass Transfer*, 52, 2009, 3187-3196.
[4] D. Pal, H. Mondal, Soret-Dufour effects on hydromagnetic non-Darcy convective-radiative heat and mass transfer over a stretching sheet in porous medium with viscous dissipation and Ohmic heating, *Journal of Applied Fluid Mechanics*, 7(3), 2014, 513–523.
[5] D. Pal, H. Mondal, MHD non-Darcy mixed convective diffusion of species over a stretching sheet embedded in a porous medium with non-uniform heat source/sink, variable viscosity and Soret effects. *Communications in Nonlinear Science and Numerical Simulation*, 17, 2012, 672-684.
[6] M.M. Rashidi, E. Momoniat, B. Rostami, Analytic approximate solutions for the MHD boundary layer viscoelastic fluid flow over continuously moving stretched surface by homotopy analysis method with two auxiliary parameters, *Journal of Applied Mathematics*, 2012, Article ID: 780415.
[7] M.M. Rashidi, E. Erfani, Analytical method for solving steady MHD and convective flow due to a rotating disk with viscous dissipation and ohmic heating, *Engineering Computations*, 29, 2012, 562–579.
[8] D. Pal, S. Chatterjee, Heat and mass transfer in mhd non-darcian flow of a micropolar fluid over a stretching sheet embedded in a porous media with non-uniform heat source and thermal radiation, *Communications in Nonlinear Science and Numerical Simulation*, 15(7), 2010, 1843-1857.
[9] R. Kandasamy, K. Periasamy, K.S. Prabhu, Effects of chemical reaction, heat and mass transfer along a wedge with heat source and concentration in the presence of suction or injection, *International Journal of Heat and Mass Transfer*, 48(7), 2005, 1388-1394.
[10] R. Kandasamy, I. Muhaimin, A.B. Khamis, Thermophoresis and variable viscosity effects on mhd mixed convective heat and mass transfer past a porous wedge in the presence of chemical reaction, *Heat and Mass Transfer*, 45(6), 2009, 703-712.
[11] D. Pal, H. Mondal, Hydromagnetic convective diffusion of species in Darcy–Forchheimer porous medium with non-uniform heat source/sink and variable viscosity, *International Communications in Heat and Mass Transfer*, 39, 2012, 913-917
[12] S. Manjunatha, B.J. Gireesha, Effects of variable viscosity and thermal conductivity on MHD flow and heat transfer of a dusty fluid, *Ain Shams Engineering Journal*, 7, 2016, 505-515.
[13] A. Pantokratoras, Further results on the variable viscosity on the flow and heat transfer to a continuous moving flat plate, *International Journal of Engineering Science*, 42, 2004, 1891-1896.
[14] S. Mukhopadhyay, G.C. Layek, Effect of thermal radiation and variable fluid viscosity on free convective and heat transfer past a porous stretching surface, *International Journal of Heat and Mass Transfer*, 21, 2008, 2167-78.
[15] M.S. Abel, P.G. Siddheshwar, M.M. Nandeppanawar, Heat transfer in a viscoelastic boundary layer flow over a stretching sheet with viscous dissipation and non-uniform heat source, *International Journal of Heat and Mass Transfer*, 50, 2007, 960-966.
[16] A. Noghrehabadi, M.R. Saffarian, R. Pourrajab, M. Ghalambaz, Entropy analysis for nanofluid flow over a stretching sheet in the presence of heat generation/absorption and partial slip. *Journal of Mechanical Science and Technology*, 27(3), 2013, 927-37.
[17] H. Sithole, H. Mondal, P. Sibanda, Entropy generation in a second grade magnetohydrodynamic nanofluid flow over a convectively heated stretching sheet with nonlinear thermal radiation and viscous dissipation, *Results in Physics*, 9, 2018, 1077-1085.
[18] N. Hidouri, M. Magherbi, H. Abbassi, A. Ben Brahim, Entropy generation in double diffusive in presence of Soret effect, *Progress in Computational Fluid Dynamics*, 5, 2007, 237-46.
[19] L. Aracely, I. Guillermo, P. Joel, M. Joel, L. Orlando, Entropy generation analysis of MHD nanofluid flow in a

porous vertical microchannel with nonlinear thermal radiation, slip flow and convective-radiative boundary conditions, *International Journal of Heat and Mass Transfer*, 107, 2017, 982-94.
[20] Kh.A. Maleque, Effects of binary chemical reaction and activation energy on mhd boundary layer heat and mass transfer flow with viscous dissipation and heat generation/ absorption, *ISRN Thermodynamics*, 2013, Article ID 284637.
[21] D. Pal, H. Mondal, Influence of chemical reaction and thermal radiation on mixed convection heat and mass transfer over a stretching sheet in Darcian porous medium with Soret and Dufour effects, *Energy Conversion and Management*, 62, 2012, 102-108
[22] M. Dhlamini, K. Peri, K. Kameswaran, P. Sibanda, S. Motsa, H. Mondal, Activation energy and binary chemical reaction effects in mixed convective nanofluid flow with convective boundary conditions, *Journal of Computational Design and Engineering*, 6(2), 2019, 149-158.
[23] F.G. Awad, S. Motsa, M. Khumalo, Heat and mass transfer in unsteady rotating fluid flow with binary chemical reaction and activation energy, *PloS One*, 9(9), 2014, 107622.
[24] H. Sithole, H. Mondal, S. Goqo, P. Sibanda, S. Motsa, Numerical simulation of couple stress nanofluid flow in magneto-porous medium with thermal radiation and a chemical reaction, *Applied Mathematics and Computation*, 339, 2018, 820-836.

ORCID iD

Hiranmoy Mondal https://orcid.org/0000-0002-9153-300X
Shweta Mishra https://orcid.org/0000-0002-5117-2051
Prabir Kumar Kundu https://orcid.org/0000-0002-8487-4893
Precious Sibanda https://orcid.org/0000-0003-2115-4642